Tip-substrate interaction in optical near-field microscopy

R. Esteban, R. Vogelgesang, and K. Kern
Max-Planck-Institut für Festkörperforschung, Stuttgart 70569, Germany
(Received 17 August 2006; revised manuscript received 21 February 2007; published 9 May 2007)

We study the tip-substrate interaction in apertureless scanning near-field optical microscopy (aSNOM) with a three-dimensional model of both near and far fields. Starting from the analytically well understood two-sphere model, we obtain a realistic tip-substrate model by continuous deformation of the upper sphere into an elongated conical tip several wavelengths long with a hemispherical apex radius of just a few nanometers. The other sphere is enlarged to represent a locally flat substrate surface below the tip apex. This adiabatic transition toward the final system helps us to understand the origin of the different contributions. We find that dielectric tips, in spite of the absence of plasmonic resonances, are quite suitable for aSNOM. This is supported by experimental results. Working with the sharpest commercially available Si tips holds promise for pushing the routinely achievable lateral resolution down to the sub-10-nm range. At 1 nm tip-substrate distance, we obtain local-field enhancements of many tens. The instantaneous, elastically backscattered intensity is calculated for variable tip-substrate distances to study demodulation at higher harmonics of an oscillating probe. We confirm that the local optical information is discriminated even against strong background signals, provided the vibration amplitude is kept small. However, this discrimination scheme is rather sensitive to crosstalk from anharmonic motion and care must be exercised in choosing appropriate experimental parameters to achieve reliable optical contrast.

DOI: 10.1103/PhysRevB.75.195410 PACS number(s): 78.67.−n, 07.79.Fc, 42.25.Fx

I. INTRODUCTION

To unravel the properties of matter at the nanometer scale, corresponding spatial resolution is indispensable. In particular, scanning near-field optical microscopes (SNOMs) provide optical information with lateral resolution well below the diffraction limit.[1,2] With the scattering-type or apertureless SNOM (aSNOM), lateral resolution around 10 nm at optical frequencies is possible, largely independent of the wavelength.[3–8] Measurements of elastic-scattering phenomena, and also Raman scattering and fluorescence, have already been demonstrated.[9–12]

In aSNOM, the substrate and a sharp tip, for example, of an atomic force microscope (AFM), are illuminated by external radiation. Two cases are often discussed. In passive mode, the apex of a nondisturbingly small or nearly transparent, optically silent tip re-scatters the near fields created at the substrate.[13–15] With an active tip, however, one usually has to consider the full interaction of the coupled tip-sample system.[16–18] This interaction can generate strong and highly confined near fields in the gap region between the tip and the substrate, which in turn leads to measurable far-field radiation. The interaction typically increases significantly for tip-substrate distances smaller than the apex radius and gives mostly information about the small volume of the surface where the confined near fields are strong. This is ultimately the cause of the high spatial resolution. For simplicity, in the following we will distinguish broadly between "near-field interaction" when referring to the local interaction just described and "background fields" from any other origin.

In a commonly used model of the aSNOM, the so-called dipole model,[5,19–22] the substrate is considered perfectly flat and the tip is approximated by a subwavelength-sized polarizable sphere of a radius equivalent to the effective curvature at the tip apex. Neglecting retardation effects and the reflection from the substrate, an incident planar wave is assumed to excite a quasistatic dipole in the spherical tip. With these simplifications, a simple analytic expression is found for the interaction of this dipole with its image dipole due to the substrate, which turns out to be strongest for polarization perpendicular to the surface. Assuming finally that the detectable far-field signal is proportional to the square of the effective polarizability of the coupled system, one appreciates how dielectric material contrast in the substrate can be obtained in aSNOM. Also, when the tip approaches the substrate to distances $d^{(ts)}$ much smaller than its radius R, a considerable nonlinear increase in the scattered field strength is predicted.

Some important aspects, however, are neglected by the quasistatic dipole model. Even for a spherical subwavelength tip, multipoles of higher order are necessary when the tip-substrate distance becomes small.[23,24] The significance of considering nonspherical tips has been underlined in numerous studies both of isolated tips[25–29] and in the presence of substrates. In the latter case, the behavior of the near-field enhancement[30–33] and particularly the detectable far fields[34] is desired to evaluate the efficacy of detection schemes for local optical contrast. As often the background fields are dominant, an adequate discrimination technique must be used to extract the near-field optical signal. One feasible scheme uses a vertically vibrating tip and demodulates this signal at higher harmonics of the oscillation frequency.[35–40]

In the present paper, we calculate near and far fields for models approaching realistic experimental conditions and study the influence of experimental parameters on the results. In particular, we simulate tips up to 1.6 μm length—corresponding to approximately three wavelengths—in the presence of a gold substrate at distances of a few to several hundred nanometers. In Ref. 41, we have already shown that the response of such long tips is not blended with antenna effects occurring in smaller tips. Silicon tips[10,30,42] do not

 ©2007 The American Physical Society

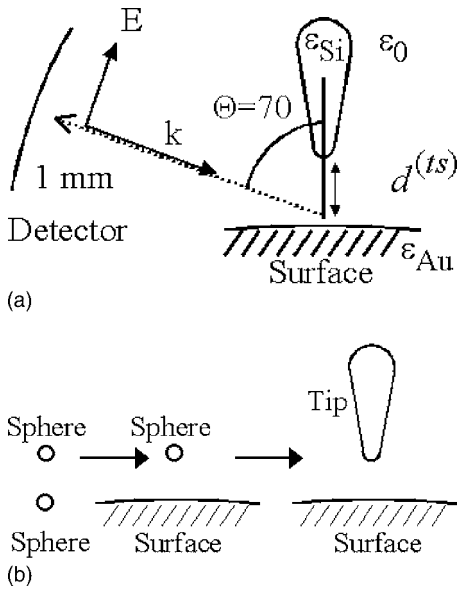

FIG. 1. (a) Illustration of the geometry used. (b) Evolution of the models simulated in the present paper, from two small spheres to a more realistic tip and substrate

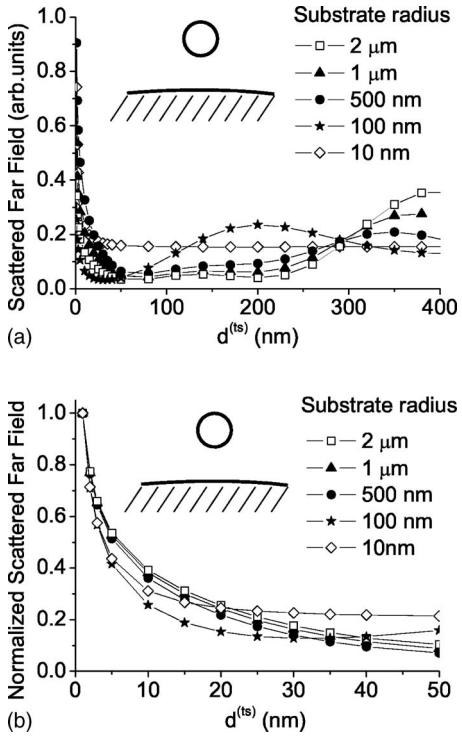

FIG. 2. (a) Scattered far field (in linear arbitrary units) as a function of tip-substrate separation for different radii of the spherical gold substrate. The tip is modeled as a silicon sphere of 10 nm radius. (b) Represents a zoom on the results, normalized to the value at $d^{(ts)}=1$ nm.

present plasmonic resonances, which are often favored to obtain high-field enhancements. Plasmonic resonances are, however, notoriously dependent on the exact shape of the tip and the influence of the substrate, and thus interpretation of the obtained images can be difficult. Measurements that do not depend on such resonances can facilitate interpretation and reproducibility of experiments.[43] Also, from a fabrication point of view, the mature silicon manufacturing technology provides off-the-shelf tips of radii smaller than 10 nm, which makes them strong candidates for the best routine lateral resolution. With the predicted far-field signals we verify that, in conjunction with appropriate demodulation, sharp silicon tips can indeed be used to detect local optical information in the far field. In addition, we show that too big an oscillation amplitude or a slightly anharmonic oscillation of the tip can significantly complicate the discrimination of the near-field signal.

II. METHOD

The simulated three-dimensional scenario is sketched in Fig. 1(a). The tips are C^1 continuous cones with a 10° half angle. They are capped by semispheres, the smaller having a radius R equal to 10 nm. The degenerate case of a 20-nm-high cone coincides with the spherical tip. The substrate is represented by spheres of increasing radius. The surrounding medium is vacuum, the tip material is silicon if not otherwise mentioned, and the substrate is gold [$\epsilon_{Si}=17.76+0.508i$, $\epsilon_{Au}=-3.95+2.58i$, $\epsilon_{Ag}=-9.448+0.209i$ (Refs. 44–46)]. We have chosen a metallic substrate because it is expected to interact strongly with the tip, a phenomenon frequently utilized in aSNOM. The incident radiation (wavelength $\lambda\sim514.5$ nm) is a planar wave or a fifth-order corrected Gaussian beam[47–49] with 500 nm waist radius focused at the sample surface, in-plane polarized with an incident angle of $\Theta=70°$ with respect to the tip axis. The focus of the Gaussian beam is centered at the substrate surface immediately below the apex of the tip. The moduli of the complex-valued near fields $|E|$ obtained are compared to the corresponding values for the planar wave and for the Gaussian beam at its focus. The scattered far field is obtained by integrating the Poynting field of the backscattered radiation over a circular detector area of numerical aperture of 0.342 situated at the far field, in particular, at 1 mm distance from the sample.

The modeling is done with the numerical platform MAX-1, which implements the multiple multipole technique[30,50,51] to solve the monochromatic Maxwell equations. This boundary-condition method considers as expansions perfect solutions in bulk material and minimizes the error in the boundary conditions between adjacent domains. It allows us to simultaneously obtain near and far fields and is well suited to tackle problems with dimensions both much bigger (tip length, substrate radius, detector distance) and smaller (tip radius, tip-substrate distance) than the wavelength. For this work, simulating a long tip in a current personal computer takes a few hours of simulation time for each considered position. We define the acceptable level of average relative error in the boundary conditions below 0.5%. The error in boundary locations other than the matching points is similarly low. Further, we verify that the admission of ~50% more parameters in the expansions does not significantly affect the results. In particular, the variation of the scattered far field is less than 1%. The demodulated results

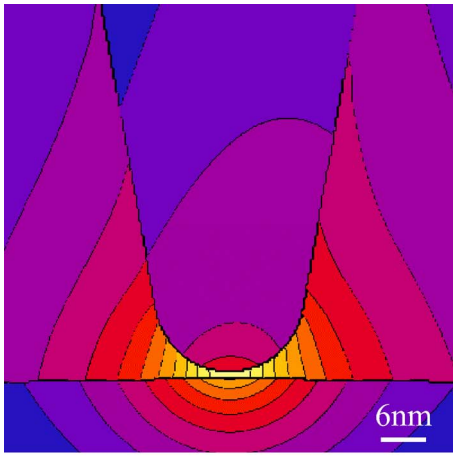

(a)

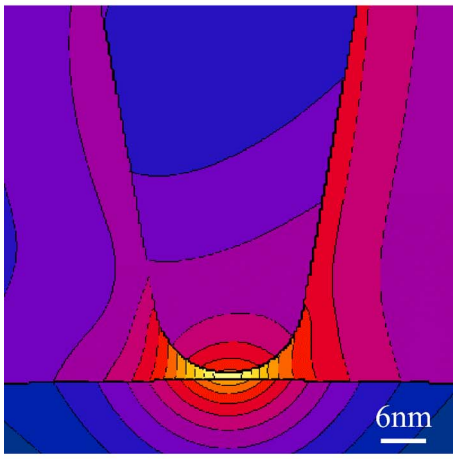

(b)

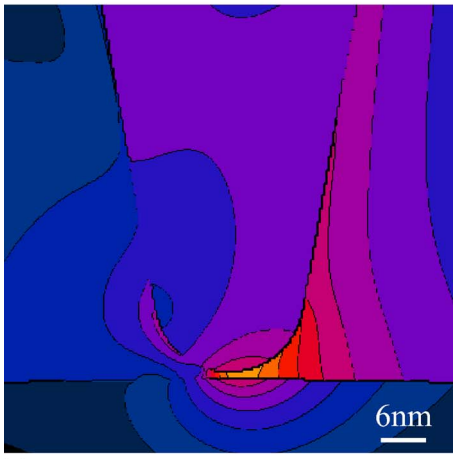

(c)

FIG. 3. (Color online) Distribution of the electric-field strength scattered by the tip-substrate system in a small area near the tip apex. The plane considered contains the axis of the tip and is parallel to the plane of incidence. The tip length is 1400 nm and the tip-substrate separation 1 nm. A logarithmic intensity scale is chosen, each isoline representing a factor of $\times 1.5$ between adjacent field strengths. (a) Silicon, (b) silver, and (c) gold tips have been considered. A near-field maximum relative to the excitation strength of ~67, ~61, and ~12, respectively, was obtained.

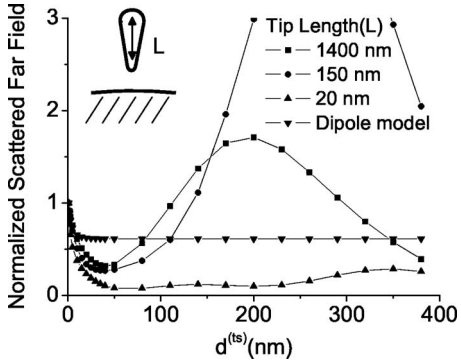

FIG. 4. The scattered far field (normalized to the 1 nm value) as a function of tip-substrate separation for silicon tips of different lengths and the prediction of the quasistatic dipole model. The substrate is a gold sphere of 2 μm diameter.

are significantly harder to converge and the variation can be bigger than 1%, but it still represents only a minor correction to the general appearance of the graphs that will be discussed.

III. TRANSITION TOWARD REALISTIC MODELS

We develop the simulations in adiabatic fashion so as to gain insight into the different signal contributions and confidence that our final model is indeed close to the experimental situation. We briefly consider the well-known system of two small and closely situated spheres (frequently used in studies of surface-enhanced Raman scattering[23]) and proceed via a "sphere over a surface" model to an "elongated tip over surface" model [Fig. 1(b)]. To avoid the strong scattering from the upper part of the tip, the long tips also require a transition from planar wave excitation toward the kind of focused illumination actually used in experiments.

When two spheres of 10 nm radius are illuminated by a planar wave and approach each other closely, they exhibit strong near-field coupling. One sphere is interpreted here as the Si tip and the other represents a Au substrate. Already in this simplified case, a clear signature of the near-field interaction is observed for $d^{(ts)} \lesssim R$ in the steep increase of the scattered far-field intensity (Fig. 2). The near field in the gap also grows for short distances, reaching at 1 nm up to more than 20-fold relative to the excitation field strength. We have calculated the fields by placing at the center of the spheres multipole expansions to describe the fields at the exterior of the spheres and Bessel expansions at the interior. It is well known that the fields scattered by an isolated small sphere in vacuum can be approximately represented by a dipole. However, the complex interactions that arise when it approaches other objects to distances less than its radius require a significant number of higher orders to achieve convergence of the numerical description. Here, for $d^{(ts)} \gtrsim 1$ nm it requires multipoles up to ~15th order. For this reason, we consider in this paper dipole approximations only briefly and we concentrate on more exact solutions of the full Maxwell equations, with expansions truncated at suitably higher multipole orders.

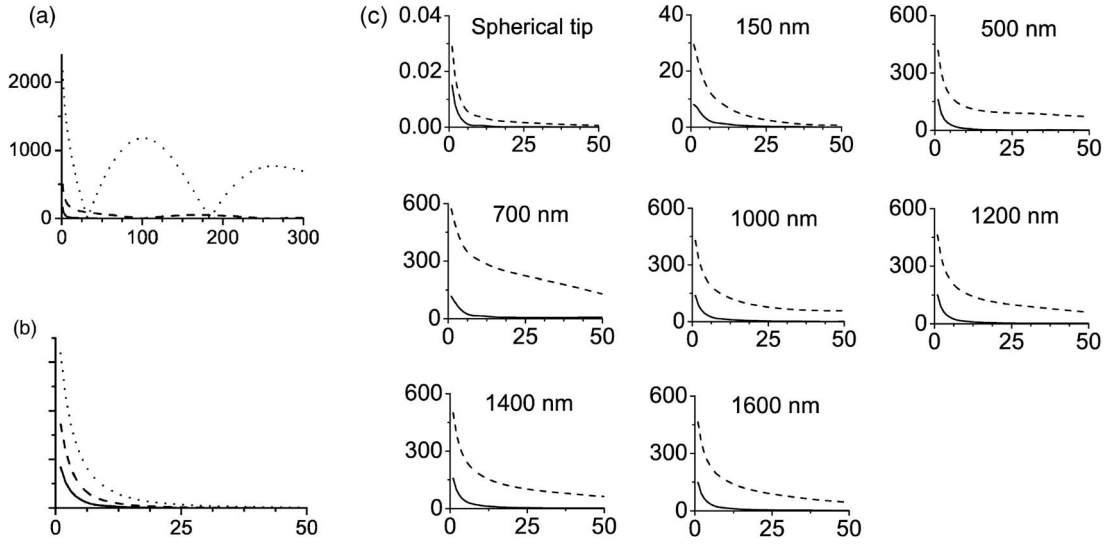

FIG. 5. Approach curves for the first (dotted), second (dashed), and third (continuous) harmonics. Plotted are the demodulated signals as functions of d_{min} for (a) a 1.4 μm tip, (b) the dipole model, and (c) tips of variable length. All results are scaled to the same arbitrary linear scale, except for the dipole model. The oscillation amplitude is 10 nm. The very weak third harmonic in (a) is better seen in (c) in the graph corresponding to 1.4 μm. For readability, only second and third harmonics are displayed in (c).

The influence of extended substrates is considered next by increasing the radius of the sphere serving as substrate up to 2 μm as shown in Fig. 2. We ignore in the rest of the paper the fields scattered by the isolated substrate and consider only the contributions due to the approaching tip. The far-field signal increases sharply with decreasing distance for $d^{(ts)} \lesssim R$, which is indicative of the near-field interaction between the tip and the substrate. As explained, this localized interaction is credited with the high achievable resolution. In addition, a modulation of the scattered far field with $d^{(ts)} \approx \lambda/2$ appears due to retardation effects. Firstly, the interference between the excitation beam and the radiation reflected by the substrate generates a standing-wave-type pattern above the substrate. Secondly, the field scattered directly by the tip and via reflections at the substrate surface can interfere constructively or destructively.

Figure 2(b) shows the behavior of the scattered far field for small $d^{(ts)}$. The results shown are normalized to the value at 1 nm distance to facilitate comparison. An asymptotic behavior for increasing substrate radius is clearly observable. When the substrate radius is several hundred nanometers big and $d^{(ts)}$ is small, the relevant surface of the substrate in the proximity of the tip apex is essentially flat and the interaction between the tip and the sphere becomes numerically equivalent to the flat substrate case. In the following, we use a substrate diameter of 2 μm.

As a last step toward our final model, we increase the length of the tip. Illuminating long tips with planar waves results in strong scattering also from the upper part of the tip.[41] A focused beam avoids this problem and also represents the experimental conditions more closely. Considering long tips affects both the near field at the apex and the scattered far fields significantly. Drastic changes in field behavior can often be associated with geometrical or antenna resonances, plasmon resonances, or the lightning rod effect.[25–28,31,52] The latter dominates for long silicon tips, with some influence of geometric resonances.[41] As expected, the fields between the tip and the substrate are highly confined and significantly stronger than the incident radiation [Fig. 3(a)]. For a 1400-nm-long tip and $d^{(ts)}=1$ nm, a full width at half maximum of $\sim$8 nm is obtained in the plane parallel to the substrate at mid distance between the tip and the substrate. The maximum near field in the gap is up to 65 times bigger than the excitation field, an excess of more than 5 times compared to the spherical tip. Concerning the far field, a small spherical tip has a scattering cross section much smaller than a realistic tip. At $d^{(ts)}=1$ nm, the scattered field intensity exhibits ratios of $\sim$34 000:1300:1, for 1400 nm, 150 nm, and spherical (20 nm) tips, respectively. For an incident power of 1 mW, the corresponding powers detected would be $\sim$1.5 μW, 60 nW, and 45 pW. Figure 4 shows the scattered far field obtained for different tip lengths, as well as the predicted values for the dipole model with the results normalized to the value at $d^{(ts)}=1$ nm for comparison. The presence of a significant background component, visible in the considerable signal for large tip-substrate distances, points to the need of an effective demodulation scheme, which we discuss next.

IV. NEAR-FIELD OPTICAL CONTRAST

A useful demodulation scheme exploits the vertical vibration of the tip in a noncontact AFM to suppress the background fields.[36,37] The measured scattered intensity oscillates with the same period as the movement of the probe, with nonzero spectral components at the higher harmonics of the vibration frequency. The amplitude of the demodulated signal can be written as

$$S_n = \frac{K}{T}\left|\int_0^T I(d^{(ts)}(t))\exp(2\pi i n f t)dt\right|, \qquad (1)$$

with

$$d^{(ts)} = d_{min} + A[1 + \cos(2\pi ft)]. \quad (2)$$

Here, S_n is the simulated signal that would be observed by a detector filtering the nth harmonic, K is a scaling factor, $d^{(ts)}$ is the tip-substrate distance, d_{min} is the minimum value of $d^{(ts)}$ during the oscillation, A is the amplitude of the vibration, and $T=f^{-1}$ are the period and inverse frequency of oscillation of the tip. I corresponds to the electrical signal generated by the detector, which for noninterferometric detection schemes is essentially proportional to the calculated scattered far-field intensity.

Approach curves, in which the demodulated signal is plotted with respect to d_{min}, are useful to show a good discrimination of the near-field components.[35,53,54] We notice from Fig. 4 that for $d^{(ts)} \gg R$ and small vibration amplitude, a low-order Taylor approximation for the scattered far field over the trajectory of the tip is sufficient, and only the lower harmonics will be of significance. However, the near-field interaction that appears at $d^{(ts)} \lesssim R$ generates a strong nonlinear dependence with d_{min} and explains significant contributions to the higher harmonics. The near-field interaction components are thus enhanced by demodulating at higher harmonics with small oscillation amplitude, and the background fields are suppressed.[39] Ideally, an approach curve will show a rapidly increasing detected signal for $d_{min} \lesssim R$, where the near-field interactions play a bigger role.

Figure 5(a) shows simulated approach curves for the 1400 nm silicon tip for distances up to 300 nm. The chosen modulation amplitude of 10 nm is sufficiently small to enhance the near-field interaction. The second and especially the third harmonic present a considerably stronger signal for small d_{min}, as desired. Not only do higher harmonics offer better signal suppression for big d_{min}, but also the demodulation intensity drops to $1/e$ of the $d_{min}=1$ nm value at shorter separations, as they enhance the high spatial frequencies of the scattered field.[38,40] The price paid is usually a smaller signal level. With the parameters used here, at $d_{min}=1$ nm and for the 1400 nm tip, the third-harmonic signal is less than 10% of that obtained with the first harmonic.

An important result of the present study concerns the influence of tip length on the demodulated results. For the first harmonic, the longer tip results (not shown here) look qualitatively similar, with some quantitative differences mostly because the background fields from the bulk of the tip are not effectively suppressed. Figures 5(b) and 5(c) show the results for the second and third harmonics for d_{min} up to 50 nm which are more relevant to near-field optical microscopy. Figure 5(c) shows that for tip lengths up to several hundred nanometers,[41] differences are manifest, clearly observed in the second harmonic. For tip lengths longer than ~ 1 μm, that is, considerably bigger than both λ and beam waist radius, the approach curves present a similar behavior. As real tips are typically many micrometers long, long tips should be considered in simulations that attempt to closely reproduce experimental results. Our results are also reassuring for experimental work, as one generally desires stable results, independent of particular tip properties, such as its length.

Another crucial parameter of the background suppression scheme is the oscillation amplitude.[33] As mentioned above,

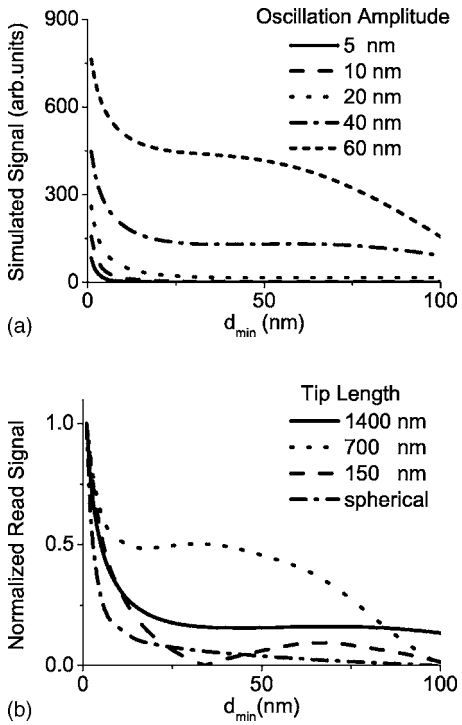

FIG. 6. Approach curves for the third harmonic (a) for a 1400 nm tip changing the oscillation amplitude and (b) for tips of different lengths and 30 nm oscillation amplitude.

higher harmonics suppress the background components if the oscillation amplitude is sufficiently small, which unfortunately also means rather low signal levels. To determine an acceptable compromise, we display the demodulated third-harmonic signal for several values of oscillation amplitude [Fig. 6(a)]. For amplitudes well above R, we find significantly worse approach curves. Figure 6(b) shows approach curves for a fixed oscillation amplitude of 30 nm and different tip lengths, normalized to the maximum value for readability. For tips shorter than ~ 1000 nm, the behavior varies appreciably, which underlines again the importance of modeling sufficiently long tips. The results for the 1400 nm in Fig. 6(b) also represent the behavior for other long tips. We have verified that both 1200- and 1600-nm-long tips result in similar approach curves.

Finally, we use the results obtained so far to study the effect of anharmonic motion of the tip. In typical AFMs, the tip oscillation is not perfectly sinusoidal but exhibits more or less strong components at the higher harmonics, with corresponding influences on experiments.[37] Consider a tip motion described by $d^{(ts)}=d_{min}+A[1+b+\cos(2\pi ft) + b\cos(3\times 2\pi ft)]$, with b being an anharmonicity parameter. Both components are considered in phase. Figure 7(a) shows the demodulated approach curves for a spherical tip, already shown in Fig. 5 to be too short to be realistic. Though some variations are discernable, qualitatively the model predicts rather similar results for anharmonic contributions up to several percent. This is not so for the more realistic 1400-nm-long tip. As shown in (b), even anharmonicity of just a few percent gives rise to noticeable qualitative differences. Thus, for an accurate estimate of the admissible an-

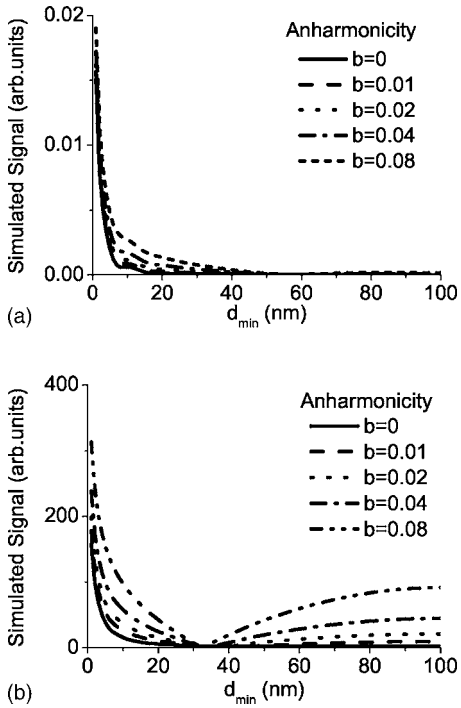

FIG. 7. Approach curves for third-harmonic demodulation with increasing anharmonicity b, modeling (a) a spherical tip and (b) a 1400-nm-long conical tip. Both tips have an apex radius of 10 nm and the modulation amplitude is 10 nm.

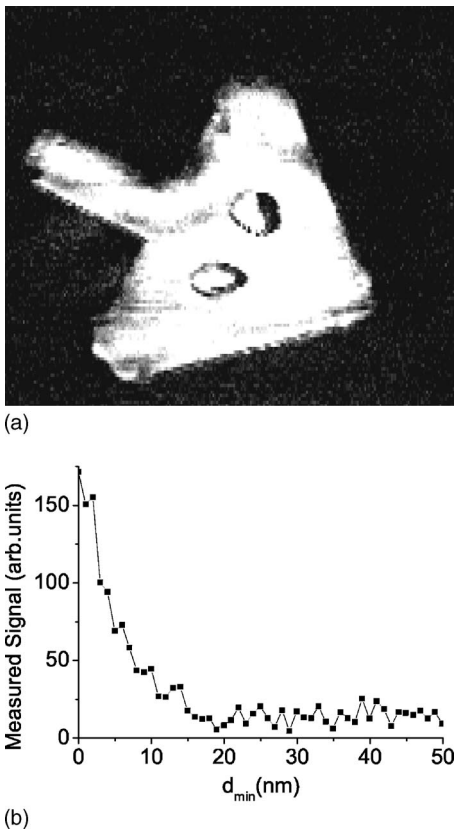

FIG. 8. Example of measured results illustrating the possibility of using silicon tips for aSNOM. The silicon tip was obtained by etching a commercial tip with HF. (a) Image of a metallic structure on glass. The glass appears black in the picture due to the much smaller level of received signal. The image size is 3×3 μm^2. (b) Measured approach curve in the third harmonic. The modulation amplitude is roughly 13 nm. In both images, $\lambda\sim820$ nm.

harmonicity, long tips are necessary in the modeling. On the experimental side, the anharmonicity should be kept below percent level or a more sophisticated scheme than a single frequency demodulation must be used to extract reliable near-field optical information.

V. DISCUSSION

This paper gives quantitative estimates of expected near-field enhancement and scattered far fields for a realistic scenario. The emphasis is put on the latter, as this is the measurable signal in aSNOM experiments. The obtained results complement experiments showing how demodulation allows discrimination of the highly localized optical information generated by the strong near-field interaction between the apex of the tip and the substrate volume immediately below.

To gain confidence in the convergence of the results, it is important to consider not only the scattered fields. Also, a well-behaved demodulated signal is crucial. The latter is harder to converge as it is sensitive to the comparatively small but fast variation of signal introduced by the near-field interaction. Even small numerical noise between adjacent points can have a measurable effect under such conditions.

Starting from simple analytical models, the transition toward realistic substrates and tips is shown. While the use of short tips may give an acceptable qualitative description of the observed phenomena, long tips together with extended substrates have to be considered to approach quantitative agreement. A spherical substrate of 2 μm diameter used in the final simulations satisfactorily represents a locally flat surface. When choosing the length of the tip to be modeled, a compromise has to be found between approaching realistic tip sizes and achieving numerical convergence in a reasonable time. For the present study, 1400-nm long tips are adequate. We verified that considering 1200- and 1600-nm-long tips does not significantly change the results presented in this paper.

Long tips are, in particular, important for including relevant phenomena neglected by spherical and small tip approximations: the increasing near fields due to the lightning rod and antenna effects and the much larger cross section. We calculate a maximum near field up to 65 times bigger than the excitation field for long tips and $d_{min}=1$ nm. The near fields are strongly confined both vertically and horizontally, and a direct study of how this translates into the good lateral resolution characteristic of aSNOM images will be treated in a future paper. For 1 mW incident power and 500 nm beam radius, ~1.5 μW scattered signal is expected. Long tips are also required to confidently study the feasibility of near-field discrimination. The described demodulation scheme significantly enhances the near-field components, though it might still be insufficient if the background signal is exceedingly high. A noninterferometric detection scheme was considered; the differences with interferometric schemes

will be studied in the future. In our simulation, second- and third-harmonic demodulations work well with amplitudes similar to the apex radius. Much larger amplitudes introduce considerably background contributions. This exemplifies how an inadequate choice of the experimental parameters, i.e., a too big amplitude or tip oscillation that is not perfectly sinusoidal, could easily overshadow the local optical information.

We have considered silicon tips, rather than the frequently used metal or metal-coated tips. The positive real part of the dielectric constant of silicon excludes enhancement effects due to plasmon coupling. Nonetheless, the lightning rod effect gives rise to strong fields near the tip apex and a clear signal from the near-field interaction can be detected. To compare, we have simulated 1.4-μm-long gold and silver tips with conditions otherwise identical to the silicon tips. The maximum of the near-field modulus for $d_{min}=1$ nm is similar for silicon and silver tips, but much weaker for gold tips (Fig. 3). We found similar trends for the respective approach curves. By optimizing the frequency and the shape of the tip, metallic tips are expected to be capable of very strong signals. However, one often has little control of these variables, and silicon tips are proved here to be a very promising alternative. Further, thanks to the highly advanced fabrication techniques, they are arguably the sharpest tips available and hold promise for the best lateral resolution. As they do not depend on resonances, they can also facilitate interpretation and reproducibility of obtained results.

The simulations presented here validate the use of silicon tip for elastic-scattering aSNOM. In Fig. 8, we illustrate experimentally that it is indeed possible to use silicon tips to obtain material contrast. An interferometric scheme was used in the experiments to enhance the signal level. An apparent difference between the signal from a metal structure and a glass substrate is observed, as the tip-substrate interaction is stronger over the metal. As expected, for aSNOM the resolution clearly is superior to the diffraction limit. Figure 8(b) shows an approach curve measured above the metal. As for the simulations, the signal increases strongly for short tip-substrate distances.

The present model constitutes a further step toward a quantitative convergence of theory and experiment in apertureless scanning near-field optical microscopy. It allows us to verify the demodulation scheme, fully accounting for the tip-substrate interaction of realistic tips. It is detailed enough to study the influence of different experimental parameters. Anharmonic tip motion or too high vibration amplitudes are found to considerably deteriorate the background suppression. Possibilities for further studies include the influence of tip and substrate material, tip apex radius, and illumination characteristics. Ultimately, a three-dimensional map of the signals generated by the tip over a structured substrate will allow us to simulate the complete imaging process and facilitate the optimization and interpretation of experiments.

[1] E. H. Synge, Philos. Mag. **6**, 356 (1928).
[2] D. W. Pohl, W. Denk, and M. Lanz, Appl. Phys. Lett. **44**, 651 (1984).
[3] F. Zenhausern, Y. Martin, and H. K. Wickramasinghe, Science **269**, 1083 (1995).
[4] Y. Inouye and S. Kawata, Opt. Lett. **19**, 159 (1994).
[5] B. Knoll and F. Keilmann, Nature (London) **399**, 134 (1999).
[6] T. Taubner, R. Hillenbrand, and F. Keilmann, J. Microsc. **210**, 311 (2003).
[7] R. Bachelot, P. Gleyzes, and A. C. Boccara, Appl. Opt. **36**, 2160 (1997).
[8] H. Sasaki and Y. Sasaki, J. Appl. Phys. **85**, 2026 (1999).
[9] A. Hartschuh, E. J. Sanchez, X. S. Xie, and L. Novotny, Phys. Rev. Lett. **90**, 095503 (2003).
[10] J. M. Gerton, L. A. Wade, G. A. Lessard, Z. Ma, and S. R. Quake, Phys. Rev. Lett. **93**, 180801 (2004).
[11] D. Hu, M. Micic, N. Klymyshyn, Y. D. Suh, and H. P. Lu, Rev. Sci. Instrum. **74**, 3347 (2003).
[12] A. Bouhelier, M. R. Beversluis, and L. Novotny, Ultramicroscopy **100**, 413 (2004).
[13] R. Carminati and J.-J. Greffet, J. Opt. Soc. Am. A **12**, 2716 (1995).
[14] O. J. F. Martin, C. Girard, and A. Dereux, J. Opt. Soc. Am. A **13**, 1801 (1996).
[15] R. Hillenbrand, F. Keilmann, P. Hanarp, D. S. Sutherland, and J. Aizpurua, Appl. Phys. Lett. **83**, 368 (2003).
[16] A. Madrazo, M. Nieto-Vesperinas, and N. García, Phys. Rev. B **53**, 3654 (1996).
[17] A. Madrazo, R. Carminati, M. Nieto-Vesperinas, and J.-J. Greffet, J. Opt. Soc. Am. A **15**, 109 (1998).
[18] M. Quinten, Appl. Phys. B: Lasers Opt. **70**, 579 (2000).
[19] R. Ruppin, Surf. Sci. **58**, 550 (1976).
[20] R. Ruppin, Surf. Sci. **127**, 108 (1983).
[21] J. Koglin, U. C. Fischer, and H. Fuchs, Phys. Rev. B **55**, 7977 (1997).
[22] S. C. Schneider, S. Grafström, and L. M. Eng, Phys. Rev. B **71**, 115418 (2005).
[23] M. Moskovits, Rev. Mod. Phys. **57**, 783 (1985).
[24] J. A. Porto, P. Johansson, S. P. Apell, and T. López-Ríos, Phys. Rev. B **67**, 085409 (2003).
[25] L. Novotny, R. X. Bian, and X. S. Xie, Phys. Rev. Lett. **79**, 645 (1997).
[26] O. J. F. Martin and C. Girard, Appl. Phys. Lett. **70**, 705 (1997).
[27] Y. C. Martin, H. F. Hamann, and H. K. Wickramasinghe, J. Appl. Phys. **89**, 5774 (2001).
[28] K. B. Crozier, A. Sundaramurthy, G. S. Kino, and C. F. Quate, J. Appl. Phys. **94**, 4632 (2003).
[29] N. Calander and M. Willander, J. Appl. Phys. **92**, 4878 (2002).
[30] J. L. Bohn, D. J. Nesbitt, and A. Gallagher, J. Opt. Soc. Am. A **18**, 2998 (2001).
[31] M. Micic, N. Klymyshyn, Y. D. Suh, and H. P. Lu, J. Phys. Chem. B **107**, 1574 (2003).
[32] H. Furokawa and S. Kawata, Opt. Commun. **148**, 221 (1998).
[33] R. Fikri, D. Barchiesi, F. H'Dhili, R. Bachelot, A. Vial, and P. Royer, Opt. Commun. **221**, 13 (2003).
[34] J. Renger, S. Grafström, L. M. Eng, and V. Deckert, J. Opt. Soc. Am. A **21**, 1362 (2004).
[35] B. Knoll and F. Keilmann, Opt. Commun. **182**, 321 (2000).

[36] M. Labardi, S. Patane, and M. Allegrini, Appl. Phys. Lett. **77**, 621 (2000).
[37] A. Bek, R. Vogelgesang, and K. Kern, Appl. Phys. Lett. **87**, 163115 (2005).
[38] J. N. Walford, J. A. Porto, R. Carminati, J.-J. Greffet, P. M. Adam, S. Hudlet, J.-L. Bijeon, A. Stashkevich, and P. Royer, J. Appl. Phys. **89**, 5159 (2001).
[39] J. L. Bijeon, P. M. Adam, D. Barchiesi, and P. Royer, Eur. Phys. J.: Appl. Phys. **26**, 45 (2004).
[40] P. M. Adam, J. L. Bijeon, G. Viardot, and P. Royer, Opt. Commun. **174**, 91 (2000).
[41] R. Esteban, R. Vogelgesang, and K. Kern, Nanotechnology **17**, 475 (2006).
[42] H. F. Hamann, M. Larbadi, S. Barzen, T. Brown, A. Gallagher, and D. J. Nesbitt, Opt. Commun. **227**, 1 (2003).
[43] A. V. Zayats, Opt. Commun. **161**, 156 (1999).
[44] D. E. Aspnes and A. A. Studna, Phys. Rev. B **27**, 985 (1983).
[45] P. B. Johnson and R. W. Christy, Phys. Rev. B **6**, 4370 (1972).
[46] C. J. Flaten and E. A. Stern, Phys. Rev. B **11**, 638 (1975).
[47] L. W. Davis, Phys. Rev. A **19**, 1177 (1979).
[48] J. P. Barton and D. R. Alexander, J. Appl. Phys. **66**, 2800 (1989).
[49] T. Evers, H. Dahl, and T. Wriedt, Electron. Lett. **32**, 1356 (1996).
[50] C. Hafner, *The Generalized Multiple Multipole Technique for Computational Electromagnetics* (Artech House, Boston, 1990).
[51] E. Moreno, D. Erni, C. Hafner, and R. Vahldieck, J. Opt. Soc. Am. A **19**, 101 (2002).
[52] J. T. Krug II, E. J. Sánchez, and X. S. Xie, J. Chem. Phys. **116**, 10895 (2002).
[53] M. B. Raschke and C. Lienau, Appl. Phys. Lett. **83**, 5089 (2003).
[54] F. Formanek, Y. De Wilde, and L. Aigouy, Ultramicroscopy **103**, 133 (2005).